Shape complexity and fractality of fracture surfaces of swelled isotactic polypropylene with supercritical carbon dioxide

Wei-Xing Zhou,* Bin Li, Tao Liu, Gui-Ping Cao, Ling Zhao, and Wei-Kang Yuan
State Key Laboratory of Chemical Engineering, East China University of Science and Technology, Shanghai 200237, China
(Received 7 January 2005; published 19 January 2006)

We have investigated the fractal characteristics and shape complexity of the fracture surfaces of swelled isotactic polypropylene Y1600 in supercritical carbon dioxide fluid through the consideration of the statistics of the regions embedded in the contours at different height of fracture landscapes (also called islands in the literature) of binary scanning electronic micrography images. The probability density functions of the areas A, perimeters L, and shape complexities C (defined by $L/2\sqrt{\pi A}$) of islands are shown to follow power laws $p(A) \sim A^{-(\mu_A+1)}$, $p(L) \sim L^{-(\mu_L+1)}$, and $p(C) \sim C^{-(\nu+1)}$, with the scaling ranges spanning over two orders. The perimeter and shape complexity scale respectively as $L \sim A^{D/2}$ and $C \sim A^q$ in two scaling regions delimited by $A \approx 10^3$. The fractal dimension and shape complexity increase when the temperature decreases. In addition, the relationships among different power-law scaling exponents μ_A, μ_B, ν, D, and q have been derived analytically, assuming that A, L, and C follow power-law distributions.

DOI: 10.1103/PhysRevE.73.011801 PACS number(s): 61.25.Hq, 05.45.Df, 68.47.Mn, 82.75.−z

I. INTRODUCTION

Polypropylene, being one of the fastest growing engineering plastics, has wide industrial and everyday life applications due to its intrinsic properties such as low density, high melting point, high tensile strength, rigidity, stress crack resistance, abrasion resistance, low creep and a surface which is highly resistance to chemical attack, and so on [1]. Impregnation of nucleating agents allows the polymer to be crystallized at a higher temperature during processing and changes a lot the mechanical and optical performance of the resultant polymer matrix [2,3]. In such nucleating agent impregnating processes, supercritical fluids are well-established swelling solvents whose strength can be tuned continuously from gaslike to liquidlike by manipulating the temperature and pressure. Especially, supercritical carbon dioxide is a good swelling agent for most polymers and will dissolve many small molecules [4–7], except for some fluoropolymers and silicones [8]. This provides the ability to control the degree of swelling in a polymer [9–11] as well as the partitioning of small molecule penetrants between a swollen polymer phase and the fluid phase [12,13].

The morphology of fracture surfaces of a material is of great concern and interest in many studies [14,15]. A frequently used tool is fractal geometry pioneered by Mandelbrot's celebrated work [16]. Specifically, fractal geometry has been widely applied to the topographical description of fracture surfaces of metals [17,18], ceramics [19–21], polymers [22–24], concretes [25–28], alloys [29–34], rocks [35–39], and many other materials. In many studies, the local roughness exponents H, which are a measure of the self-affinity of the profile perpendicular to the propagation direction of the crack, are reported to be close to 0.8 and are therefore regarded as universal [29,40–42]. On the other hand, many different approaches have been adopted in the determination of fractal dimensions D of fracture surfaces and the estimated fractal dimensions from different materials vary from case to case and are not universal, where $D=2-H$ was used when compared to Bouchaud's universal local roughness exponent [43]. It is noteworthy that there is no direct relation between the fractal dimension of rough surface and the local roughness exponent of profiles perpendicular to the crack propagation direction, since the two quantities concern different geometric objects.

Concerning the fractal characterization of the fracture surfaces of polypropylene, it was found that the fractal dimension of the fracture surfaces is less than 2.12 [23]. In this paper, we investigate the shape complexity and fractality of fracture surfaces of nucleating agents impregnated isotactic polypropylene (Y1600) swelled with supercritical carbon dioxide based on the area-perimeter relationship [16,17,44]. We shall see that the fractal dimension of the fracture surface of supercritical dioxide swelled polypropylene is much higher than that without swelling and decreases with increasing temperature.

II. EXPERIMENT

The isotactic polypropylene (Y1600) powder we have used has an average diameter of 3 to 4 mm. Fifteen grams of isotactic polypropylene powder was melted in an oven at 200 °C and then made into film with a thickness of 0.3 mm by using a press machine with a pressure of 0.5 Giga Newtown. The size of the standard film samples was 1×3 mm^2 and are refluxed with acetone for 24 h to remove the impurities, and then annealed at 200 °C for 2 h.

The specimens are then swelled with supercritical carbon dioxide. The schematic flow chart of the experimental apparatus of swelling is illustrated in Fig. 1. The experimental apparatus consists mainly of a gas cylinder, a gas booster, a digital pressure gauge, an electrical heating bath, and valves and fittings of different kinds. The system was cleaned thoroughly using suitable solvents and dried under vacuum. Iso-

*Electronic address: wxzhou@moho.ess.ucla.edu

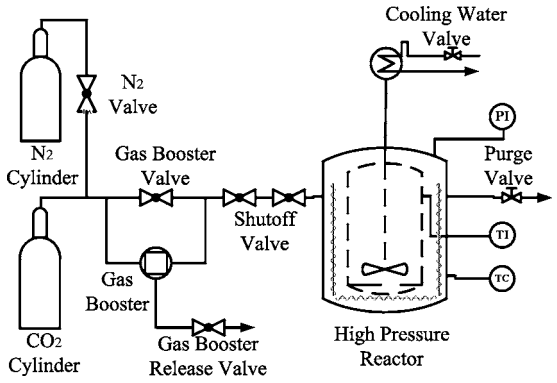

FIG. 1. Schematic flowchart of the experimental apparatus of the swelling of isotactic polypropylene with supercritical carbon dioxide.

tactic polypropylene films marked from 1 to 12 were placed in the high pressure cell together with the desired amount (1 wt %) of nucleating agent (NA21). The system was purged with CO_2 and after the system had reached the desired temperature and thermal equilibrium, CO_2 was charged until the desired pressure was reached. The impregnation process lasted for 4 h and then depressurized the CO_2 from the high pressure cell rapidly. Then the vessel was cooled and opened, and the specimens were taken out for analysis. All of the metallic parts in contact with the studied chemicals were made of stainless steel. The apparatus was tested up to 35 MPa. The total volume of the system is 500 mL. The swelled polypropylene films with a notch at the center of each film were merged in liquid nitrogen for a few minutes and the fracture surfaces were obtained by bending, resulting in a mode I failure.

The swelling experiments were performed at fixed pressure of 7.584 MPa and at four different temperatures of $T=60$, 80, 100, and 120 °C. For each sample, we took ten scanning electronic micrography (SEM) pictures at magnification of 5000 or 10 000. The pictures have 256 gray levels. Due to the nature of area-perimeter approach, the results are irrelevant to the magnification [16]. A gray-level picture was transformed into a black-and-white image for a given level set ϵ according to the criterion that a pixel is black if its gray level is larger than 256ϵ and is white otherwise. The resultant binary image has many black islands (i.e., the regions embedded by contours at a given height of the fracture surface

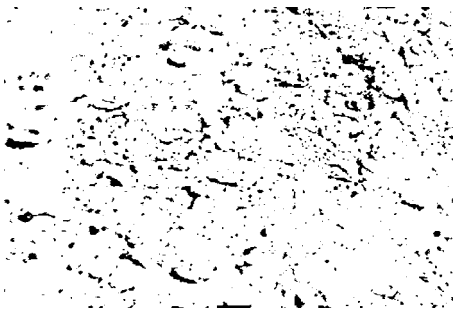

FIG. 2. Image of the recognized islands from a typical SEM picture of swelled isotactic polypropylene impregnated with NA21 at a level set of 0.7.

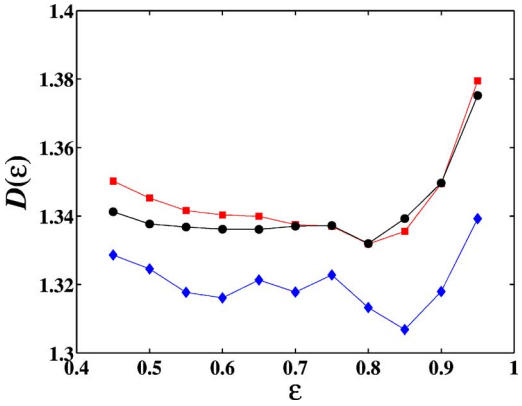

FIG. 3. (Color online) Functional area-perimeter analysis of three SEM images from experiments with $T=80$ °C.

landscape). A typical binary image of islands is shown in Fig. 2. In our calculations, we have used 11 level sets from 0.45 to 0.95 spaced by 0.05 for each SEM picture.

III. FRACTALITY AND SHAPE COMPLEXITY

A. Functional area-perimeter analysis

If an island is fractal, its area A and perimeter L follow a simple relation,

$$L^{1/D} \sim A^{1/2}, \tag{1}$$

where D is the fractal dimension describing the wiggliness of the perimeter. For $D=1$, the perimeter of the island is smooth. For $D=2$, the perimeter becomes more and more contorted to fill the plane. This area-perimeter relation (1) can also be applied to many islands when they are self-similar in the sense that the ratio of $L^{1/D}$ over $A^{1/2}$ is constant for different islands [16]. It has been used to investigate the geometry of satellite- and radar-determined cloud and rain regions by drawing A against L for different regions in a log-log plot [44]. The slope of the straight line obtained by performing a linear regression of the data gives $2/D$.

For many kinds of surface, the fractal dimensions vary with height thresholds, which can be illustrated by the functional box-counting method [45]. The theory has been worked out [46] with direct confirmation from experiments, such as laboratory rough surfaces [35] and topography surfaces [47–50], and simulations [51] as well. This multifractal nature was also observed in our experimental results. Figure 3 plots the fractal dimension $D(\epsilon)$ as a function of the height threshold ϵ using functional area-perimeter analysis. We find that $D(\epsilon)$ is not independent of the threshold ϵ, especially for large and small threshold values. However, we focus on the fractal aspect in our ensuing analysis, which amounts to taking a canonical averaging view of the fracture surface topology.

When D is interpreted as the fractal dimension of the perimeter, relation (1) amounts to assume that the fractal dimension if any of the area is two [46]. When both the perimeter and the area are fractal with fractal dimensions D_L and $D_A \neq 2$, then a box-counting estimation of the fractals dimensions gives

$$A(r) = \left(\frac{R}{r}\right)^{D_A} r^2 \tag{2}$$

and

$$L(r) = \left(\frac{R}{r}\right)^{D_L} r. \tag{3}$$

Eliminating r, we obtain

$$A \propto L^{(2-D_A)/(1-D_L)}. \tag{4}$$

Comparing Eqs. (4) and (1), we have

$$D = \frac{2(1-D_L)}{2-D_A}. \tag{5}$$

In this case, D is actually not a fractal dimension, but some scaling exponent relating D_A and D_L. Actually, we have performed boxing-counting analysis on the area and do not observe power law between the number of boxes and the resolution r.

B. Scaling between area and perimeter

Based on the area-perimeter relation, we plotted for each temperature L against A for all islands identified at different level sets. The resultant scatter plot for a given temperature shows nice collapse to a straight line. The four slopes are $D=1.34\pm0.08$ for $T=60$ °C, $D=1.32\pm0.07$ for $T=80$ °C, $D=1.31\pm0.08$ for $T=100$ °C, and $D=1.28\pm0.09$ for $T=120$ °C, respectively. The errors were estimated by the rms of the fit residuals.

However, a closer investigation of the scatter plots shows that there are two scaling regions with a kink at around $A=1000$. To have a better view angle, we adopt an averaging technique for both A and L. We insert $n-2$ points in the interval $[\min(A),\max(A)]$ resulting in $\min(A)=a_0<a_1<a_2<\cdots<a_n=\max(A)$ so that a_i's are logarithmically spaced. We can identify all islands whose areas fall in the interval $[a_i,a_{i+1})$. The geometric means of L and A are calculated for these islands, denoted as $\langle L\rangle$ and $\langle A\rangle$. The calculated means $\langle L\rangle$ and $\langle A\rangle$ are plotted in Fig. 4. The two scaling regions are fitted, respectively, with two straight lines and we have $D_1=1.42\pm0.06$ for $T=60$ °C, $D_1=1.33\pm0.06$ for $T=80$ °C, $D_1=1.33\pm0.07$ for $T=100$ °C, and $D_1=1.30\pm0.05$ for $T=120$ °C, in the first region that $\langle A\rangle<1000$ and $D_2=1.96\pm0.07$ for $T=60$ °C, $D_2=1.89\pm0.24$ for $T=80$ °C, $D_2=2.15\pm0.11$ for $T=100$ °C, and $D_2=2.07\pm0.14$ for $T=120$ °C in the second region that $\langle A\rangle>1000$.

It is very interesting to notice that $L\propto A$ for large areas. Under the assumption that the islands are fractals, this relation can be interpreted that the perimeters of the large islands are so wiggly that they can fill the plane. However, there are simple models that can deny this assumption of self-similarity. Consider that we have a set of striplike islands with length l and width w. We have $L=2(l+w)$ and $A=lw$. When w is fixed and $l\gg w$, it follows that $L\propto A$. This simple model can indeed explain the current situation. For cracked polypropylene, there are big striplike ridges in the intersection whose surface is relatively smooth. For small islands, the fractal nature is more sound.

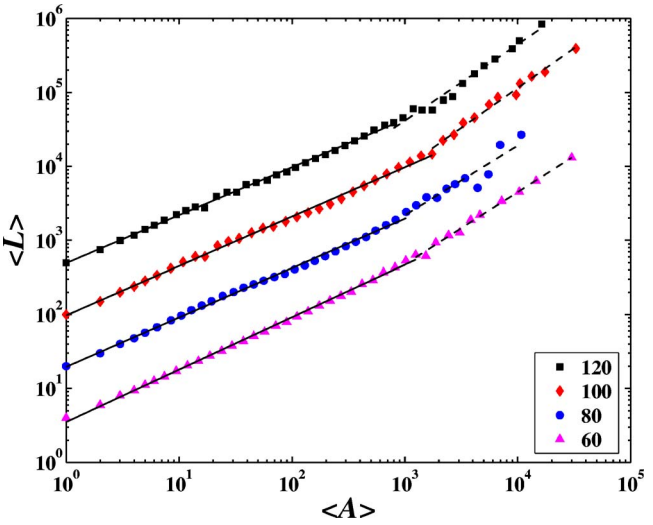

FIG. 4. (Color online) Plots of $\langle L\rangle$ with respect to $\langle A\rangle$ at different temperatures. The plots are translated vertically for clarity. We note that $\langle L\rangle=4$ when $\langle A\rangle=1$ in all four plots.

According to the additive rule of codimensions of two intersecting independent sets, the fractal dimension of the surface is $D_s=D_1+1$ [16]. Therefore $D_s=2.42\pm0.06$ for $T=60$ °C, $D_s=2.33\pm0.06$ for $T=80$ °C, $D_s=2.33\pm0.07$ for $T=100$ °C, and $D_s=2.30\pm0.05$ for $T=120$ °C. We see that the fractal dimension D_s increases with decreasing temperature. In other words, with the increase of temperature, the surface becomes smoother.

C. Rank-ordering statistics of area and perimeter

In order to estimate the probability distribution of a physical variable empirically, several approaches are available. For a possible power-law distribution with fat tails, cumulative distribution or log-binning technique are usually adopted. A similar concept to the complementary distribution, called rank-ordering statistics [52], has the advantage of easy implementation, no information loss, and being less noisy.

Consider n observations of variable x sampled from a distribution whose probability density is $p(x)$. Then the complementary distribution is $P(y>x)=\int_x^\infty p(y)dy$. We sort the n observations in nonincreasing order such that $x_1\geqslant x_2\geqslant\cdots\geqslant x_R\geqslant\cdots\geqslant x_n$, where R is the rank of the observation. It follows that $nP(x\geqslant x_R)$ is the expected number of observations larger than or equal to x_R, that is

$$nP(x\geqslant x_R)=R. \tag{6}$$

If the probability density of variable x follows a power law that $p(x)\sim x^{-(1+\mu)}$, then the complementary distribution $P(x)\sim x^{-\mu}$. An intuitive relation between x_R and R follows

$$x_R\sim R^{-1/\mu}. \tag{7}$$

A rigorous expression of Eq. (7) by calculating the most probable value of x_R from the probability that the Rth value equals x_R gives [52]

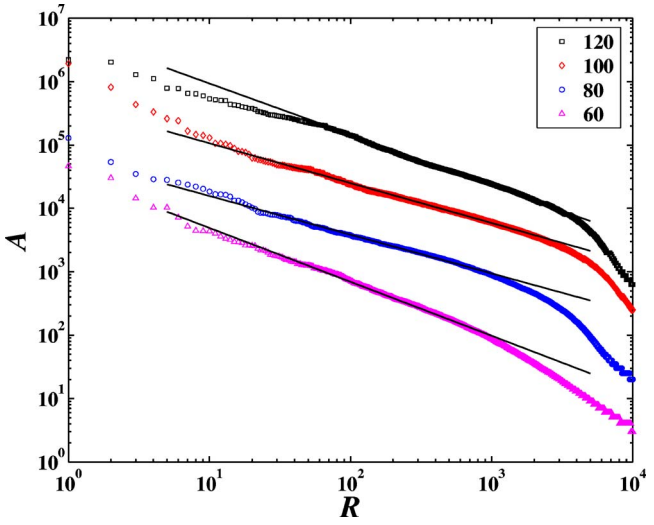

FIG. 5. (Color online) Log-log plot of the rank-ordered areas A at different temperatures shown in the legend. The plots are translated vertically for clarity. The solid lines are linear fits to the data at $59 \leqslant R \leqslant 3890$ for $T=120$ °C, $10 \leqslant R \leqslant 1995$ for $T=100$ °C, $22 \leqslant R \leqslant 1000$ for $T=80$ °C, and $8 \leqslant R \leqslant 800$ for $T=60$ °C, respectively.

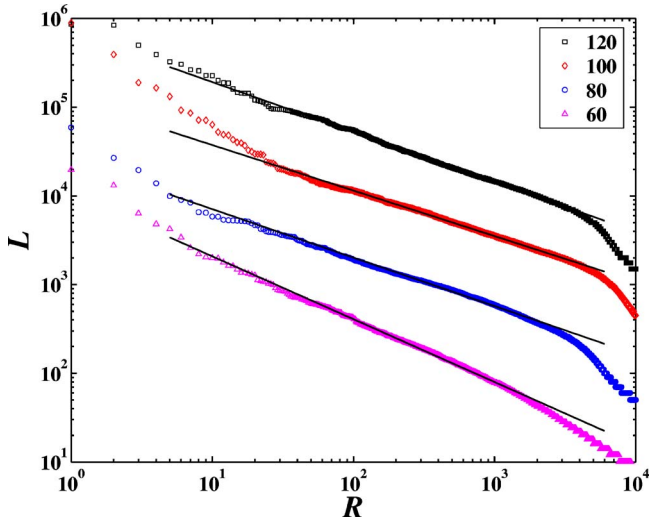

FIG. 6. (Color online) Log-log plot of the rank-ordered perimeters L at different temperatures marked in the legend. The plots are translated vertically for clarity. The solid lines are linear fits to the data at $5 \leqslant R \leqslant 3890$ for $T=120$ °C, $24 \leqslant R \leqslant 3000$ for $T=100$ °C, $16 \leqslant R \leqslant 2000$ for $T=80$ °C, and $10 \leqslant R \leqslant 1500$ for $T=60$ °C, respectively.

$$x_R \sim \left(\frac{\mu n+1}{\mu R+1}\right)^{1/\mu}, \tag{8}$$

when $\mu R \gg 1$ or equivalently $1 \ll R \leqslant N$, we retrieve Eq. (7). A plot of $\ln x_R$ as a function of $\ln R$ gives a straight line with slope $-1/\mu$ with deviations for the first few ranks if x is distributed according to a power law of exponent μ.

We note that the rank-ordering statistics is nothing but a simple generalization of Zipf's law [16,52,53] and has wide applications, such as in linguistics [54], the distribution of large earthquakes [55], time-occurrences of extreme floods [56], to list a few. More generally, rank-ordering statistics can be applied to probability distributions other than power laws, such as exponential or stretched exponential distributions [57], normal or log-normal distributions [52], and so on.

Figure 5 illustrates the log-log plots of the rank-ordered areas A at different temperatures. There is clear power-law dependence between A and its rank R with the scaling ranges spanning over about two decades. Least-squared linear fitting gives $1/\mu_A=0.80\pm0.05$, $1/\mu_A=0.63\pm0.02$, $1/\mu_A=0.61\pm0.03$, and $1/\mu_A=0.85\pm0.04$ with decreasing temperatures, where the errors are estimated by the rms of the fit residuals. Using $\sigma_{\mu_A}=\sigma_{1/\mu_A}\mu_A^2$, we obtain the power-law exponents $\mu_A=1.24\pm0.08$, $\mu_A=1.59\pm0.06$, $\mu_A=1.64\pm0.09$, and $\mu_A=1.18\pm0.05$ with decreasing temperatures.

Figure 6 shows the log-log plots of the rank-ordered perimeters L at different temperatures. There are also clear power-law relations between L and its rank R whose scaling ranges spanning over about three orders. Least-squared linear fitting gives $1/\mu_L=0.56\pm0.02$,$1/\mu_L=0.51\pm0.01$,$1/\mu_L=0.55\pm0.03$, and $1/\mu_L=0.71\pm0.03$ with decreasing temperatures. We thus obtain the power-law exponents $\mu_L=1.78\pm0.07$, $\mu_L=1.95\pm0.05$, $\mu_L=1.83\pm0.12$, and $\mu_L=1.41\pm0.06$ with decreasing temperatures. It is noteworthy that the scaling ranges of the rank-ordering of both A and P are well above two decades broader than most other experiments with scaling ranges centered around 1.3 orders of magnitude and spanning mainly between 0.5 and 2.0 [58,59].

Assuming that $p(A) \sim A^{-(\mu_A+1)}$ and $p(L) \sim L^{-(\mu_L+1)}$, we can estimate the fractal dimension D in Eq. (1) according to the relation $p(A)dA=p(L)dL$ such that

$$D = 2\mu_A/\mu_L. \tag{9}$$

The four estimated values of D using this relation (9) are 1.67, 1.79, 1.63, and 1.40 with increasing temperature. The discrepancy of D from D_1 is remarkable (15%, 25%, 18%, and 7%, accordingly). The source of this discrepancy is threefold. First, the power-law distributions of A and L have cutoffs at both ends of small and large values so that the derivation of Eq. (9) is not rigorous. Second, the determination of the scaling ranges may cause errors. Third, the scaling ranges of the three power laws are not consistent with each other. Fourth, this may stem from the fact that a fractal view of the surface is rough and thus call for further multifractal analysis.

D. Shape complexity

To quantify the shape complexity of an irregular fractal object, besides the fractal dimension, there are other relevant measures related to the fractal nature [60,61]. For a d-dimensional hypersphere, its surface and volume are related by

$$S_{d,sph} = \frac{1}{k_d} V_{d,sph}^{(d-1)/d}, \tag{10}$$

where

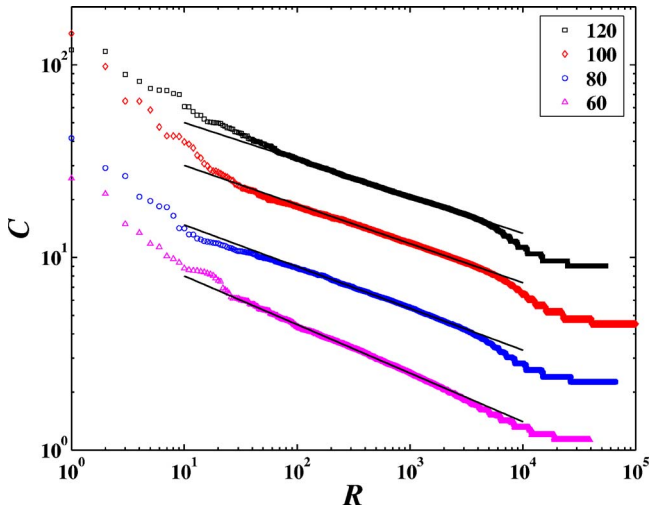

FIG. 7. (Color online) Log-log plot of the rank-ordered shape complexity C at different temperatures. The plots are translated vertically for clarity. The solid lines are linear fits to the data at $40 \leqslant R \leqslant 3890$ for $T=120$ °C, $24 \leqslant R \leqslant 5000$ for $T=100$ °C, $40 \leqslant R \leqslant 3000$ for $T=80$ °C, and $25 \leqslant R \leqslant 1500$ for $T=60$ °C, respectively.

$$k_d = \frac{\Gamma^{1/2}(1+d/2)}{d\pi^{1/2}}. \tag{11}$$

Since a hypersphere has the maximal enclosed volume among the objects with a given surface S_d, we have

$$S_d \geqslant \frac{1}{k_d} V_d^{(d-1)/d}. \tag{12}$$

Then the following dimensionless ratio

$$C_d \triangleq \frac{k_d S_d}{V_d^{(d-1)/d}} \tag{13}$$

describes the irregularity or complexity of the investigated object [60]. It follows that $1 \leqslant C_d \leqslant \infty$. The limits are reached at $C_d=1$ for hyperspheres and $C_d=\infty$ for fractals. For real fractal objects, sometimes known as prefractals [62], the scaling range is not infinite. The shape complexity C_d is thus finite. In the case of $d=2$, we have

$$1 \leqslant C \triangleq \frac{L}{2\pi^{1/2}A^{1/2}} \leqslant \infty. \tag{14}$$

This dimensionless measure of shape complexity has been applied to a scalar field of concentration in turbulent jet at high Reynolds numbers [60,63].

In Fig. 7 is shown the log-log plot of the rank-ordered shape complexity C at different temperatures. The power-law dependence $C \sim R^{-1/\nu}$ implies a power-law probability density of shape complexity, that is

$$p(C) \sim C^{-(\nu+1)}. \tag{15}$$

We find that $\nu=3.97\pm0.11$ for $T=60$ °C, $\nu=4.61\pm0.17$ for $T=80$ °C, $\nu=4.93\pm0.20$ for $T=100$ °C, and $\nu=5.22\pm0.17$ for $T=120$ °C. The mean logarithmic complexity $\langle \ln C \rangle = 1/(\nu-1)$ [60] is calculated to be 0.34, 0.28, 0.25, and 0.24

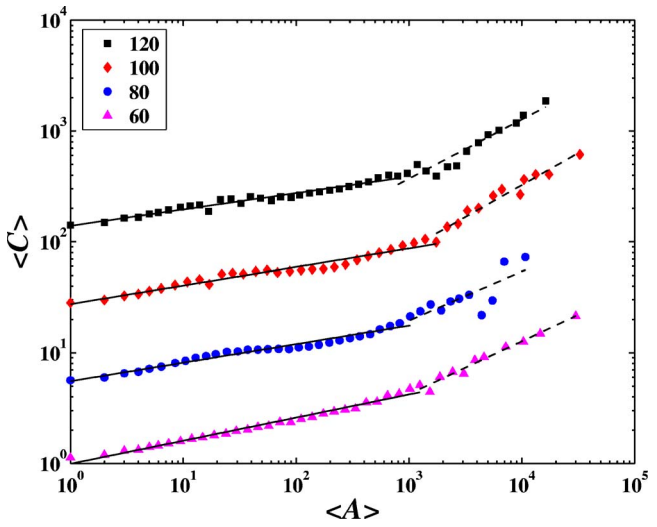

FIG. 8. (Color online) Plots of $\langle C \rangle$ with respect to $\langle A \rangle$ at different temperatures. The plots are translated vertically for clarity. We note that $\langle C \rangle = 2/\pi^{1/2}$ when $\langle A \rangle = 1$ in all four plots.

with increasing temperature. In other words, the shape complexity of the islands decreases with increasing temperature. This is consistent with the fact that D decreases with increasing temperature.

Following the procedure in Sec. III B, we calculate the means, $\langle A \rangle$ and $\langle C \rangle$. The results are shown in Fig. 8. Again, we see two scaling regions guided by straight lines fitted to the data

$$C \sim A^q. \tag{16}$$

The slopes are, respectively, $q_1=0.21$ for $T=60$ °C, $q_1=0.17$ for $T=80$ °C, $q_1=0.17$ for $T=100$ °C, and $q_1=0.15$ for $T=120$ °C, in the first region that $\langle A \rangle < 1000$ and $q_2=0.54$ for $T=60$ °C, $q_2=0.58$ for $T=80$ °C, $q_2=0.44$ for $T=100$ °C, and $q_2=0.48$ for $T=120$ °C in the second region that $\langle A \rangle > 1000$.We have verified that $q_i=(D_i-1)/2$ with $i=1,2$ holds exactly for all cases, which is nothing but a direct consequence of the combination of Eqs. (1) and (14).

Similarly, we can derive the relationship among q, D, μ_A, and ν as follows:

$$\nu = 2\mu_A/(D-1) = \mu_A/q. \tag{17}$$

Again, the discrepancy between the fitted ν values and those estimated indirectly from Eq. (17) is remarkable (38%, 48%, 53%, and 30%), which can also be resorted to similar reasoning.

IV. CONCLUSION

We have investigated the fractal characteristics of the fracture surfaces of swelled isotactic polypropylene Y1600 impregnated with nucleating agent NA21 through consideration of the statistics of the islands in binary images. At a given temperature, the distributions of area and perimeter of the islands are found to follow power laws spanning over two decades of magnitude, via rank-ordering statistics. The

well-established power-law scaling between area and perimeter shows the overall self-similarity among islands when $A < 10^3$. This shows that the fracture surface is self-similar. For large islands, the fractal dimension is estimated to be close to 2 which can be explained by the fact that most of the large islands are strip-shaped. The fracture surface is rougher at low temperature with larger fractal dimension.

We have also investigated the shape complexity of the fracture surfaces using a dimensionless measure C. The distribution of shape complexity is also found to follow a power law spanning over two orders of magnitude. The shape complexity increases when the island is larger. There are two power-law scaling ranges between C and A delimited around $A = 10^3$, corresponding to the two-regime area-perimeter relationship. The exponent q_1 serves as an inverse measure of overall shape complexity, which is observed to increase with temperature. This is consistent with the change of fractal dimension at different temperatures.

Furthermore, the relationships among different power-law scaling exponents of the probability distributions (μ_A, μ_B, and ν), of area-perimeter relation (D), and of complexity-area relation (q) have been derived analytically. However, these relations hold only when the probability distributions of A, L, and C follow the power laws exactly. In the present case, we observed remarkable discrepancy between numerical and analytical results.

ACKNOWLEDGMENTS

The isotactic polypropylene (Y1600) powder was kindly provided by the Plastics Department of Shanghai Petrochemical Company and the nucleating agent, NA21, was kindly supplied by Asahi Denka Co, Ltd. Apparatus. This work was jointly supported by NSFC/PetroChina through a major project on multiscale methodology (No. 20490200).

[1] *Polypropylene Handbook*, edited by E. P. Moore (Hanser Gardner, New York, 1996).
[2] T. Xu, H. Lei, and C.-S. Xie, Mater. Des. **24**, 227 (2003).
[3] J. O. Iroh and J. P. Berry, Eur. Polym. J. **32**, 1425 (1996).
[4] J. S. Chiou, J. W. Barlow, and D. R. Paul, J. Appl. Polym. Sci. **30**, 2633 (1985).
[5] Y. Kamiya, T. Hirose, Y. Naito, and K. Mizoguchi, J. Polym. Sci., Part B: Polym. Phys. **26**, 159 (1988).
[6] A. R. Berens, G. S. Huvard, R. W. Korsmeyer, and F. W. Kunig, J. Appl. Polym. Sci. **46**, 231 (1992).
[7] Y. Kamiya, K. Mizoguchi, K. Terada, Y. Fujiwara, and J. S. Wang, Macromolecules **31**, 472 (1998).
[8] W. H. Tuminello, G. T. Dee, and M. A. McHugh, Macromolecules **28**, 1506 (1995).
[9] G. K. Fleming and W. J. Koros, Macromolecules **19**, 2285 (1986).
[10] D. S. Pope and W. J. Koros, J. Polym. Sci., Part B: Polym. Phys. **34**, 1861 (1996).
[11] P. D. Condo, S. R. Sumpter, M. L. Lee, and K. P. Johnston, Ind. Eng. Chem. Res. **35**, 1115 (1996).
[12] M. F. Vincent, S. G. Kazarian, and C. A. Eckert, AIChE J. **43**, 1838 (1997).
[13] S. G. Kazarian, M. F. Vincent, B. L. West, and C. A. Eckert, J. Supercrit. Fluids **13**, 107 (1998).
[14] G. P. Cherepanov, A. S. Balankin, and V. S. Ivanova, Eng. Fract. Mech. **51**, 997 (1995).
[15] J. Fineberg and M. Marder, Phys. Rep. **313**, 1 (1999).
[16] B. B. Mandelbrot, *The Fractal Geometry of Nature* (W. H. Freeman, New York, 1983).
[17] B. Mandelbrot, D. Passoja, and A. Paullay, Nature (London) **308**, 721 (1984).
[18] U. Wendt, K. Stiebe-Lange, and M. Smid, J. Microsc. **207**, 169 (2002).
[19] J. J. Mecholsky, D. E. Passoja, and K. S. Feinberg-Ringel, J. Am. Ceram. Soc. **72**, 60 (1989).
[20] J. Y. Thompson, K. J. Anusavice, B. Balasubramaniam, and J. J. Mecholsky, J. Am. Ceram. Soc. **78**, 3045 (1995).
[21] A. Celli, A. Tucci, L. Esposito, and P. Carlo, J. Eur. Ceram. Soc. **23**, 469 (2003).
[22] C. T. Chen and J. Runt, Polym. Commun. **30**, 334 (1989).
[23] J. Yu, T. Xu, Y. Tian, X. Chen, and Z. Luo, Mater. Des. **23**, 89 (2002).
[24] F. Lapique, P. Meakin, J. Feder, and T. Jøssang, J. Appl. Polym. Sci. **86**, 973 (2002).
[25] L. Dougan and P. Addison, Cem. Concr. Res. **31**, 1043 (2001).
[26] Y. Wang and S. Diamond, Cem. Concr. Res. **31**, 1385 (2001).
[27] M. A. Issa, M. A. Issa, M. S. Islam, and A. Chudnovsky, Eng. Fract. Mech. **70**, 125 (2003).
[28] A. Yan, K. -R. Wu, D. Zhang, and W. Yao, Cem. Concr. Compos. **25**, 153 (2003).
[29] E. Bouchaud, G. Lapasset, and J. Planés, Europhys. Lett. **13**, 73 (1990).
[30] C. Shek, G. Lin, K. Lee, and J. Lai, J. Non-Cryst. Solids **224**, 244 (1998).
[31] X. Wang, H. Zhou, Z. H. Wang, M. S. Tian, Y. S. Liu, and Q. P. Kong, Mater. Sci. Eng., A **266**, 250 (1999).
[32] V. I. Betekhtin, P. N. Butenko, V. L. Gilyarov, V. E. Korsukov, A. S. Luk'yanenko, B. A. Obidov, and V. E. Khartsiev, Tech. Phys. Lett. **28**, 26 (2002).
[33] F. Paun and E. Bouchaud, Int. J. Fract. **121**, 43 (2003).
[34] A. Eftekhari, Appl. Surf. Sci. **220**, 343 (2003).
[35] J. Schmittbuhl, F. Schmitt, and C. Scholz, J. Geophys. Res. **100**, 5953 (1995).
[36] J. M. Lòpez and J. Schmittbuhl, Phys. Rev. E **57**, 6405 (1998).
[37] H.-P. Xie, H.-Q. Sun, Y. Ju, and Z. -G. Feng, Int. J. Solids Struct. **38**, 5765 (2001).
[38] T. Babadagli and K. Develi, Theor. Appl. Fract. Mech. **39**, 73 (2003).
[39] H. W. Zhou and H. Xie, Surf. Rev. Lett. **10**, 751 (2003).
[40] E. Bouchaud, J. Phys.: Condens. Matter **9**, 4319 (1997).
[41] E. Bouchaud, Surf. Rev. Lett. **10**, 797 (2003).
[42] G. Mourot, S. Morel, E. Bouchaud, and G. Valentin, Phys. Rev. E **71**, 016136 (2005).
[43] S. G. Wang, Physica B **348**, 183 (2004).

[44] S. Lovejoy, Science **216**, 185 (1982).
[45] S. Lovejoy, D. Schertzer, and A. A. Tsonis, Science **235**, 1036 (1987).
[46] S. Lovejoy and D. Schertzer, in *Non-Linear Variability in Geophysics: Scaling and Fractals* (Kluwer, Boston, 1991), pp. 111–144.
[47] S. Lovejoy and D. Schertzer, Phys. Canada 46, 62 (1990).
[48] H. -P. Xie, J. -A. Wang, and E. Stein, Phys. Lett. A **242**, 41 (1998).
[49] J. S. Gagnon, S. Lovejoy, and D. Schertzer, Europhys. Lett. **62**, 801 (2003).
[50] S. Stach, J. Cybo, J. Cwajna, and S. Roskosz, Mater. Sci. **23**, 577 (2005).
[51] S. Stach, J. Cwajna, S. Roskosz, and J. Cybo, Mater. Sci. **23**, 567 (2005).
[52] D. Sornette, *Critical Phenomena in Natural Sciences—Chaos, Fractals, Self-organization and Disorder: Concepts and Tools*, 1st ed. (Springer, Berlin, 2000).
[53] G. K. Zipf, *Human Behavior and The Principle of Least Effort* (Addison-Wesley Press, Reading, MA, 1949).
[54] B. B. Mandelbrot, Word **10**, 1 (1954).
[55] D. Sornette, L. Knopoff, Y. Kagan, and C. Vanneste, J. Geophys. Res., [Solid Earth] **101**, 13883 (1996).
[56] A. Mazzarella and F. Rapetti, J. Hydrol. **288**, 264 (2004).
[57] J. Laherrere and D. Sornette, Eur. Phys. J. B **2**, 525 (1998).
[58] O. Malcai, D. A. Lidar, O. Biham, and D. Avnir, Phys. Rev. E **56**, 2817 (1997).
[59] D. Avnir, O. Biham, D. Lidar, and O. Malcai, Science **279**, 39 (1998).
[60] H. J. Catrakis and P. E. Dimotakis, Phys. Rev. Lett. **80**, 968 (1998).
[61] J. Kondev, C. L. Henley, and D. G. Salinas, Phys. Rev. E **61**, 104 (2000).
[62] P. S. Addison, Fractals **8**, 147 (2000).
[63] H. J. Catrakis, R. C. Aguirre, J. Ruiz-Plancarte, and R. D. Thayne, Phys. Fluids **14**, 3891 (2002).